Double-Input Interval Type-2 Fuzzy Logic Controllers: Analysis and Design

Andriy Sarabakha[1,2], Changhong Fu[1,2] and Erdal Kayacan[1]
[1]School of Mechanical and Aerospace Engineering
[2]ST Engineering-NTU Corporate Laboratory
Nanyang Technological University, 50 Nanyang Avenue, 639798, Singapore
Email: andriy001@e.ntu.edu.sg, {changhongfu, erdal}@ntu.edu.sg

Abstract—A significant number of investigations of type-1 and type-2 fuzzy logic controllers have revealed their exceptional ability to capture uncertainties in complex and nonlinear systems, particularly in real-time control applications. However, regardless of being type-1 or type-2, fuzzy logic controller design is still a complicated task due to the lack of a closed form solution of the output and an interpretable relationship between the control output and fuzzy logic controller design parameters, such as center or width of the membership functions. To simplify the design procedure further, we think every attempt to obtain such interpretable relationships is worthwhile. Accordingly, this paper aims to design a double-input interval type-2 fuzzy PID controller and obtain interpretable relationships between the input and the output of the controller. Thereafter, we deploy the novel design for the control of a Y6 coaxial tricopter unmanned aerial vehicle. Simulation results, which are realised in robot operating system (ROS) using C++ and Gazebo environment, are found to tally with the theoretical analysis and claims in the paper.

I. INTRODUCTION

Fuzzy logic controllers (FLCs) have become one of the most popular model-free control structures, and have been proposed as an alternative approach to conventional model-based controllers when it is challenging to obtain the precise mathematical model of the system [1], [2]. This is due to several characteristics of FLCs, *inter-alia*, improving the robustness and flexibility of the nonlinear control system in the presence of uncertainties and external disturbances using expert knowledge throughout the controller design. Many researchers recently put significant attention toward more advanced forms of FLCs, such as type-2 FLCs (T2-FLCs) [3], [4]. T2-FLCs can be used to handle uncertainties better in the system, e.g., noisy measurements, due to the additional degree of freedom provided by the footprint of uncertainty (FOU) in their fuzzy sets (FSs) [5]. The interval T2-FLCs (IT2-FLCs) have received more consideration because the mathematics that is needed for IT2-FLCs – primarily interval arithmetic – is much simpler than that of general T2-FLCs [6]. The use of IT2-FLC helps to decrease the computation time which is a big advantage in real-time on-board control applications [7]. Thus, several studies have been presented to analyse the effect of the FOU on the type-2 fuzzy mapping (FM) [8]. To generate the desired FM, evolutionary algorithms have been employed [9]. The main drawback of these approaches is the lack of understanding of how the FOU parameters affect the robustness and performance of the IT2-FLC [10]. Undoubtedly, the derivation

of FM for IT2-FLC in an analytical form can provide an efficient tool to examine the IT2-FLC. The FM for single input IT2-FLCs (SI-IT2-FLCs) has been recently derived and analysed in [11]. However, the analytical derivation of the FM was restricted to single input structure only, and for double input IT2-FLCs (DI-IT2-FLC) is still missing in the literature.

In this paper, we have explicitly derived an FM for DI-IT2-FLC, composed of nine rules commonly preferred in the literature, to investigate its robustness based on its analytical representation. The proposed analytical closed form relationship between the input and the output of the fuzzy controller provides an explanation on the role of the FOU parameters. Furthermore, the presented analytical design method allows to generate control surfaces (CSs) by altering only the size of FOU without any optimisation procedure. Moreover, it is shown that various controllers with more aggressive or less aggressive behaviour can be developed by tuning only two FOU parameters, thereby providing a certain degree of robustness and stability to the system.

In this paper, double input interval type-2 fuzzy PID (DI-IT2-FPID) controllers, which make use of DI-IT2-FLCs, are elaborated in terms of their design simplicity as well as interpretability. A realistic application of DI-IT2-FPID is shown for the trajectory tracking problem of Y6 coaxial tricopter unmanned aerial vehicle (UAV). Unlike the conventional robotic applications, such as robotic manipulators, where the system model perfectly describes the overall system dynamics, UAVs are subject to inevitable uncertainties, e.g., global positioning system (GPS) and inertial measurement unit (IMU) measurements, wind and gust conditions. In this paper, our main goal is to give a novel analysis for DI-IT2-FLC rather than compare its performance with its type-1 counterpart. Hence, different parameter settings (PSs) for the DI-IT2-FPID controller are tested to investigate their control performances. To the best of our knowledge, for the first time, an FM for DI-IT2-FLC is derived, analysed, implemented in robot operating system (ROS) and tested in Gazebo simulator.

This paper is organised as follows. Section II briefly reviews the definition of IT2-FLC and, in particular, DI-IT2-FLC. In Section III, an FM for DI-IT2-FLC is derived and analysed. Section IV provides dynamical simulations with Y6 coaxial tricopter UAV in order to prove the theoretical claims. Finally, Section V closes this paper with conclusions and future works.

II. Double Input Interval Type-2 FLC

In this section, we introduce some important definitions [2] for IT2-FLC, which will be used in the rest of this paper.

Definition 1: An interval type-2 FS (IT2-FS) $\tilde{A}$ is described by an interval type-2 membership function (MF), $\mu_{\tilde{A}}(\sigma, u) = 1$, for example in Fig. 1a, where $\sigma \in \Sigma$ and $u \in U_\sigma \subseteq [0,1]$, i.e.:

$$\tilde{A} = \{(\sigma, u, 1) \mid \forall \sigma \in \Sigma, \forall u \in U_\sigma \subseteq [0,1]\}. \tag{1}$$

Definition 2: Uncertainty in each FS $\tilde{A}$ consists of a bounded region (grey area in Fig. 1a) which is the FOU and it is a union of all $\mu_{\tilde{A}}(\sigma, u)$, i.e.:

$$\text{FOU}(\tilde{A}) = \bigcup_{\sigma \in \Sigma} U_\sigma. \tag{2}$$

Definition 3: The MF which upper bounds $\text{FOU}(\tilde{A})$ (red lines in Fig. 1a) is called upper MF (UMF) of $\tilde{A}$ and is denoted $\overline{\mu}_{\tilde{A}}(\sigma), \forall \sigma \in \Sigma$; while the MF which lower bounds $\text{FOU}(\tilde{A})$ (blue lines in Fig. 1a) is called lower MF (LMF) of $\tilde{A}$ and is denoted $\underline{\mu}_{\tilde{A}}(\sigma), \forall \sigma \in \Sigma$, i.e.:

$$\begin{cases} \overline{\mu}_{\tilde{A}}(\sigma) = \overline{\text{FOU}(\tilde{A})} & \forall \sigma \in \Sigma \\ \underline{\mu}_{\tilde{A}}(\sigma) = \underline{\text{FOU}(\tilde{A})} & \forall \sigma \in \Sigma. \end{cases} \tag{3}$$

Note that for an IT2-FS, $U_\sigma = [\underline{\mu}_{\tilde{A}}(\sigma), \overline{\mu}_{\tilde{A}}(\sigma)], \forall \sigma \in \Sigma$ [12].

Definition 4: For DI-IT2-FLC, the i-th rule $R_i \in \mathbf{R}$, $i = 1, \ldots, N$, can be expressed as an IF $-$ THEN statement, i.e.:

$$R_i : \text{IF } \sigma_1 \text{ is } \tilde{A}_{1,i} \text{ and } \sigma_2 \text{ is } \tilde{A}_{2,i}, \text{ THEN } \varphi \text{ is } C_i. \tag{4}$$

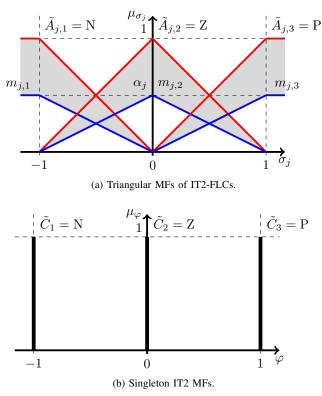

(a) Triangular MFs of IT2-FLCs.

(b) Singleton IT2 MFs.

Fig. 1. Antecedent and consequent MFs of IT2-FLC.

Definition 5: For DI-IT2-FLC, the firing set of the i-th rule $F_i(\boldsymbol{\sigma}) = [\underline{f}_i(\boldsymbol{\sigma}); \overline{f}_i(\boldsymbol{\sigma})]$ is

$$\begin{cases} \overline{f}_i(\boldsymbol{\sigma}) = \overline{\mu}_{A_{1,i}}(\sigma_1) \times \overline{\mu}_{A_{2,i}}(\sigma_2) \\ \underline{f}_i(\boldsymbol{\sigma}) = \underline{\mu}_{A_{1,i}}(\sigma_1) \times \underline{\mu}_{A_{2,i}}(\sigma_2). \end{cases} \tag{5}$$

Definition 6: An FM from $\boldsymbol{\sigma} \in \mathbb{R}^n$ to $\varphi \in \mathbb{R}$ is a function $\varphi(\boldsymbol{\sigma}) : \mathbb{R}^n \to \mathbb{R}$.

Once we determine the rules in (4), a DI-T2-FLC can be seen as a quantitative FM from crisp inputs $\boldsymbol{\sigma} = \begin{bmatrix} \sigma_1 & \sigma_2 \end{bmatrix}^T$ to crisp output φ. In our case, the antecedent MFs are defined as triangular IT2-FSs, as depicted in Fig. 1a. The conventional way to represent triangular IT2-FSs is

$$\overline{\mu}_{\tilde{A}_i}(\sigma_j) = \begin{cases} \frac{\sigma_j - a_{i-1}}{a_i - a_{i-1}} & , a_{i-1} \le \sigma_j \le a_i \\ \frac{a_{i+1} - \sigma_j}{a_{i+1} - a_i} & , a_i < \sigma_j \le a_{i+1} \\ 0 & , \sigma_j < a_{i-1}, a_{i+1} < \sigma_j \end{cases} \tag{6}$$

$$\underline{\mu}_{\tilde{A}_{j,k}}(\sigma_j) = m_{j,k} \overline{\mu}_{\tilde{A}_{j,k}}(\sigma_j), \tag{7}$$

where a_k are the cores of the triangular MFs and $m_{j,k}$ represent the height of the lower MFs [11]. However, for our analysis, we need complex symbolic computations, therefore, a new equivalent algebraic definition of (6) is needed [13]:

$$\overline{\mu}_{\tilde{A}_{j,k}}(\sigma_j) = \max\left(\min\left(\frac{\sigma_j - a_{i-1}}{a_i - a_{i-1}}, \frac{a_{i+1} - \sigma_j}{a_{i+1} - a_i}\right), 0\right), \tag{8}$$

in which min and max functions are also redefined as:

$$\begin{cases} \min(a,b) = \frac{a+b-|a-b|}{2} \\ \max(a,b) = \frac{a+b+|a-b|}{2}. \end{cases} \tag{9}$$

In this paper, symmetrical MFs are employed to simplify the design complexity. In this context, we define $m_{j,k}$ as follows:

$$m_{j,1} = m_{j,2} = m_{j,3} = \alpha_j. \tag{10}$$

Thus, α_j is the only parameter to be tuned for each input σ_j. The consequent MFs are singleton and depicted in Fig. 1b.

The structure of DI-IT2-FPID controller is shown in Fig. 2. The DI-IT2-FPID inherits DI-IT2-FLC with α_1 and α_2. Here, the scaling factors k_p and k_d are defined such that the inputs e and $\dot{e}$ are normalized to the domain of the antecedent MFs, i.e., $[-1, 1]$. Thus, the error e and the derivative of the error $\dot{e}$ are converted after normalisation into σ_1 and σ_2, respectively, which are the inputs to the DI-IT2-FLC. Thereafter, its output φ is converted into the control signal v. Thus, in this control structure, only four parameters have to be tuned, i.e., α_1, α_2, k_1 and k_2, and the number of parameters is the same as for SI-IT2-FPID in [11].
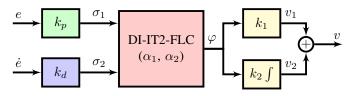

Fig. 2. Structure of DI-IT2-FPID controller.

III. DERIVATION AND ANALYSIS OF DI-IT2-FLC

A. Derivation of DI-IT2-FLC

Let the defuzified output of IT2-FLC be, as in [2]:

$$\varphi(\boldsymbol{\sigma}) = \frac{\varphi_L(\boldsymbol{\sigma}) + \varphi_R(\boldsymbol{\sigma})}{2}, \tag{11}$$

where φ_L and φ_R are the left and right end points of the type-reduced set and they can be computed with centroid type reduction technique using Karnik-Mendel algorithm [14]:

$$\varphi_L(\boldsymbol{\sigma}) = \frac{\sum_{i=1}^{L} \overline{f}_i(\boldsymbol{\sigma}) C_i + \sum_{i=L+1}^{N} \underline{f}_i(\boldsymbol{\sigma}) C_i}{\sum_{i=1}^{L} \overline{f}_i(\boldsymbol{\sigma}) + \sum_{i=L+1}^{N} \underline{f}_i(\boldsymbol{\sigma})}$$
$$\varphi_R(\boldsymbol{\sigma}) = \frac{\sum_{i=1}^{R} \underline{f}_i(\boldsymbol{\sigma}) C_i + \sum_{i=R+1}^{N} \overline{f}_i(\boldsymbol{\sigma}) C_i}{\sum_{i=1}^{R} \underline{f}_i(\boldsymbol{\sigma}) + \sum_{i=R+1}^{N} \overline{f}_i(\boldsymbol{\sigma})}, \tag{12}$$

in which R and L are the switching points. Using common and typical nine rules in Table I [15], three different cases for L and R can be found, i.e., $\{L=3, R=3\}$, $\{L=3, R=6\}$ and $\{L=6, R=6\}$. For each case we will have a region (Ω_1, Ω_2, Ω_3) on the $[\sigma_1 \times \sigma_2]$ plane, as shown in Fig. 3. Hence, Ω_1, Ω_2 and Ω_3 are analytically defined as:

$$\Omega_1 = \left\{ \{\sigma_1, \sigma_2\} \in [-1,1]^2 \mid \sigma_2 \geq -1, \sigma_2 \leq \omega_{12}(\sigma_1) \right\}$$
$$\Omega_2 = \left\{ \{\sigma_1, \sigma_2\} \in [-1,1]^2 \mid \sigma_2 > \omega_{12}(\sigma_1), \sigma_2 < \omega_{23}(\sigma_1) \right\}$$
$$\Omega_3 = \left\{ \{\sigma_1, \sigma_2\} \in [-1,1]^2 \mid \sigma_2 \geq \omega_{23}(\sigma_1), \sigma_2 \leq 1 \right\}, \tag{13}$$

where ω_{12} and ω_{23} are contours which separate Ω_1 from Ω_2 and Ω_2 from Ω_3, respectively. Each region is associated with an FM, i.e., $\varphi_1(\boldsymbol{\sigma})$, $\varphi_2(\boldsymbol{\sigma})$ and $\varphi_3(\boldsymbol{\sigma})$, respectively. Therefore, $\varphi(\boldsymbol{\sigma})$ can be decomposed using (11):

$$\varphi(\boldsymbol{\sigma}) = \begin{cases} \varphi_1(\boldsymbol{\sigma}) = \frac{\varphi_{L=3}(\boldsymbol{\sigma}) + \varphi_{R=3}(\boldsymbol{\sigma})}{2}, & \boldsymbol{\sigma} \in \Omega_1 \\ \varphi_2(\boldsymbol{\sigma}) = \frac{\varphi_{L=3}(\boldsymbol{\sigma}) + \varphi_{R=6}(\boldsymbol{\sigma})}{2}, & \boldsymbol{\sigma} \in \Omega_2 \\ \varphi_3(\boldsymbol{\sigma}) = \frac{\varphi_{L=6}(\boldsymbol{\sigma}) + \varphi_{R=6}(\boldsymbol{\sigma})}{2}, & \boldsymbol{\sigma} \in \Omega_3. \end{cases} \tag{14}$$

The formulation in (14) reduces the design of DI-IT2-FLC into a generation of CS. As shown in Fig. 1a, DI-IT2-FLC employs fully overlapping IT2-FSs. Consequently, it is
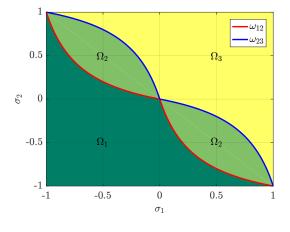
Fig. 3. Three control regions of DI-IT2-FM and their contours.

Derivative error, σ_2	Proportional error, σ_1		
	(N)egative	(Z)ero	(P)ositive
(N)egative	(N)egative	(N)egative	(Z)ero
(Z)ero	(N)egative	(Z)ero	(P)ositive
(P)ositive	(Z)ero	(P)ositive	(P)ositive

guaranteed that crisp inputs σ_j always belong to at most two successive IT2-FSs. Therefore, we are able to find FM $\varphi(\boldsymbol{\sigma})$ in a closed form. Once we derive $\varphi_{L=3}(\boldsymbol{\sigma})$, $\varphi_{L=6}(\boldsymbol{\sigma})$, $\varphi_{R=3}(\boldsymbol{\sigma})$ and $\varphi_{R=6}(\boldsymbol{\sigma})$ with (12):

$$\varphi_{L=3}(\boldsymbol{\sigma}) = \frac{\sigma_1(\sigma_2+1) - \sigma_1\sigma_2 + \sigma_2(\sigma_1+1)}{\alpha_1\alpha_2(\sigma_1+1)(\sigma_2+1) - \sigma_1 - \sigma_2(\sigma_1+1)}$$
$$\varphi_{L=6}(\boldsymbol{\sigma}) = \frac{\alpha_1\alpha_2\sigma_2 - \alpha_1\alpha_2\sigma_1(\sigma_2-1)}{(\sigma_1-1)(\sigma_2-1) + \alpha_1\alpha_2(\sigma_1+\sigma_2-\sigma_2\sigma_1)}$$
$$\varphi_{R=3}(\boldsymbol{\sigma}) = \frac{\alpha_1\alpha_2\sigma_1 + \alpha_1\alpha_2\sigma_2(\sigma_1+1)}{(\sigma_1+1)(\sigma_2+1) - \alpha_1\alpha_2(\sigma_1\sigma_2+\sigma_1+\sigma_2)}$$
$$\varphi_{R=6}(\boldsymbol{\sigma}) = \frac{\sigma_1(1-\sigma_2) + \sigma_1\sigma_2 - \sigma_2(1-\sigma_1)}{\alpha_1\alpha_2(\sigma_1-1)(\sigma_2-1) - \sigma_1 - \sigma_2(\sigma_1-1)}, \tag{15}$$

$\varphi_1(\boldsymbol{\sigma})$, $\varphi_2(\boldsymbol{\sigma})$ and $\varphi_3(\boldsymbol{\sigma})$ can be computed with (14):

$$\varphi_1(\boldsymbol{\sigma}) = \frac{1}{2} \frac{\alpha_1\alpha_2(\sigma_1\sigma_2 - \sigma_1 - \sigma_2)}{(\sigma_1-1)(\sigma_2-1) + \alpha_1\alpha_2\sigma_1 - \alpha_1\alpha_2\sigma_2(\sigma_1-1)}$$
$$+ \frac{1}{2} \frac{\sigma_1\sigma_2 - \sigma_1 - \sigma_2}{\sigma_1 + \sigma_2 - \sigma_1\sigma_2 + \alpha_1\alpha_2(\sigma_1-1)(\sigma_2-1)}$$
$$\varphi_2(\boldsymbol{\sigma}) = \frac{1}{2} \frac{\sigma_2(\sigma_1+1) - \alpha_1\alpha_2\sigma_1(\sigma_2-1)}{\sigma_2(\sigma_1+1) - \alpha_1\alpha_2\sigma_1 - \alpha_1\alpha_2(\sigma_1+1)(\sigma_2-1)}$$
$$- \frac{1}{2} \frac{\sigma_1(\sigma_2-1) - \alpha_1\alpha_2\sigma_2(\sigma_1+1)}{\sigma_1(\sigma_2-1) + \alpha_1\alpha_2\sigma_2 - \alpha_1\alpha_2(\sigma_1+1)(\sigma_2-1)}$$
$$\varphi_3(\boldsymbol{\sigma}) = \frac{1}{2} \frac{\alpha_1\alpha_2(\sigma_1+\sigma_2-\sigma_1\sigma_2)}{(\sigma_1-1)(\sigma_2-1) + \alpha_1\alpha_2\sigma_1 - \alpha_1\alpha_2\sigma_2(\sigma_1-1)}$$
$$- \frac{1}{2} \frac{\sigma_1\sigma_2 - \sigma_1 - \sigma_2}{\sigma_1 + \sigma_2 - \sigma_1\sigma_2 + \alpha_1\alpha_2(\sigma_1-1)(\sigma_2-1)}. \tag{16}$$

Finally, ω_{12} and ω_{23} are computed by using the definition $\omega_{12} = \left\{ \boldsymbol{\sigma} \in [-1,1]^2 \mid \varphi_{R=3}(\boldsymbol{\sigma}) = \varphi_{R=6}(\boldsymbol{\sigma}) \right\}$ and $\omega_{23} = \left\{ \boldsymbol{\sigma} \in [-1,1]^2 \mid \varphi_{L=3}(\boldsymbol{\sigma}) = \varphi_{L=6}(\boldsymbol{\sigma}) \right\}$:

$$\omega_{12}(\sigma_1) = \begin{cases} \frac{-\sigma_1}{\sigma_1 + \alpha_1\alpha_2 - \alpha_1\alpha_2\sigma_1}, & \sigma_1 < 0 \\ \frac{-\alpha_1\alpha_2\sigma_1}{\sigma_1 - \alpha_1\alpha_2\sigma_1 + 1}, & \sigma_1 \geq 0 \end{cases}$$
$$\omega_{23}(\sigma_1) = \begin{cases} \frac{-\sigma_1}{\alpha_1\alpha_2 - \sigma_1 + \alpha_1\alpha_2\sigma_1}, & \sigma_1 < 0 \\ \frac{-\alpha_1\alpha_2\sigma_1}{\alpha_1\alpha_2\sigma_1 - \sigma_1 + 1}, & \sigma_1 \geq 0. \end{cases} \tag{17}$$

Thus, instead of using DI-IT2-FLC as a black box, we can use an explicit representation of DI-IT2-FLC in (14), i.e., $\varphi(\boldsymbol{\sigma})$.

The control surfaces, which map the two inputs σ_1 and σ_2 to the output φ, are shown in Fig. 4. It can be observed that it is possible to easily generate different types of control surfaces by simply tuning the two FOU parameters α_1 and α_2.

Remark 1: For illustrative simplicity we assume $\alpha_1 = \alpha_2$. On the other hand, as can be seen from (16) and (17), they are utterly independent.
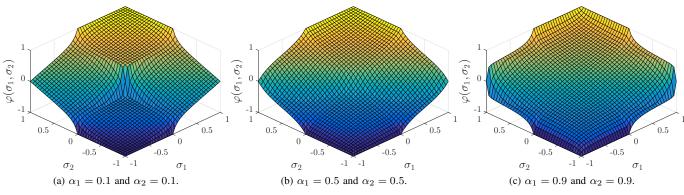
Fig. 4. Illustration of the control surfaces with different values of α_1 and α_2.

(a) $\alpha_1 = 0.1$ and $\alpha_2 = 0.1$.   (b) $\alpha_1 = 0.5$ and $\alpha_2 = 0.5$.   (c) $\alpha_1 = 0.9$ and $\alpha_2 = 0.9$.

B. Analysis of DI-IT2-FLC

The gradient of $\varphi(\boldsymbol{\sigma})$ is $\delta(\boldsymbol{\sigma}) = \nabla\varphi(\boldsymbol{\sigma})$. We define the aggressiveness of a CS as the value of $\delta(\boldsymbol{\sigma})$ in the neighbourhood of $(0,0)$ and in the direction of the unit vector $\hat{\mathbf{w}} = \begin{bmatrix} \frac{1}{\sqrt{2}} & \frac{1}{\sqrt{2}} \end{bmatrix}^T$:

$$\delta^T(0,0)\hat{\mathbf{w}} = \frac{\sqrt{2}}{2}\left(\alpha_1\alpha_2 + \frac{1}{\alpha_1\alpha_2}\right). \tag{18}$$

Therefore, if we decrease α_1 and/or α_2, the DI-IT2-FLC will have a more aggressive behaviour around $(0,0)$; while increasing α_1 and/or α_2, the response of DI-IT2-FLC around $(0,0)$ will be smoother, as can be seen also from Fig. 5.

Remark 2: If $\varphi(\boldsymbol{\sigma})$ is continuous for all α_1 and α_2 in $(0,1]$, then $\varphi(\boldsymbol{\sigma})$ can be used as a control function.

Lemma 1: If $\varphi_{L=3}(\boldsymbol{\sigma})$, $\varphi_{L=6}(\boldsymbol{\sigma})$, $\varphi_{R=3}(\boldsymbol{\sigma})$ and $\varphi_{R=6}(\boldsymbol{\sigma})$ denote the left and right FMs of the type-reduced set, ω_{12} is the switching border between $\varphi_{R=3}(\boldsymbol{\sigma})$ and $\varphi_{R=6}(\boldsymbol{\sigma})$, and ω_{23} is the switching border between $\varphi_{L=3}(\boldsymbol{\sigma})$ and $\varphi_{L=6}(\boldsymbol{\sigma})$, then

$$\begin{cases} \varphi_{L=3}(\boldsymbol{\sigma}) = \varphi_{L=6}(\boldsymbol{\sigma}) = 0 & \forall \boldsymbol{\sigma} \mid \sigma_2 = \omega_{23}(\sigma_1) \\ \varphi_{R=3}(\boldsymbol{\sigma}) = \varphi_{R=6}(\boldsymbol{\sigma}) = 0 & \forall \boldsymbol{\sigma} \mid \sigma_2 = \omega_{12}(\sigma_1). \end{cases} \tag{19}$$
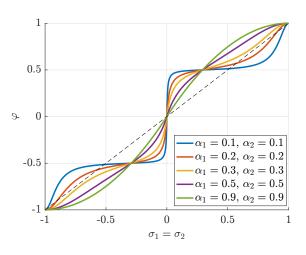

Fig. 5. Sections of control surfaces with different values of α_1 and α_2.

Proof: Substituting (17) in (15), we can check that $\varphi_{R=3}(\sigma_1, \omega_{12}(\sigma_1)) = 0$, $\varphi_{R=6}(\sigma_1, \omega_{12}(\sigma_1)) = 0$, $\varphi_{L=3}(\sigma_1, \omega_{23}(\sigma_1)) = 0$ and $\varphi_{L=6}(\sigma_1, \omega_{23}(\sigma_1)) = 0$. ∎

Theorem 1: If $\varphi(\boldsymbol{\sigma})$ denotes FM of DI-IT2-FLC, then $\varphi(\boldsymbol{\sigma})$ is a continuous FM in the region $[-1,1]^2$ with respect to its input variable $\boldsymbol{\sigma}$, i.e., $\varphi \in \mathcal{C}^0([-1,1]^2)$.

Proof: We can observe from (15) that $\varphi_{L=3}(\boldsymbol{\sigma})$, $\varphi_{L=6}(\boldsymbol{\sigma})$, $\varphi_{R=3}(\boldsymbol{\sigma})$ and $\varphi_{R=6}(\boldsymbol{\sigma})$ have no vertical asymptotes in their domains of definition, i.e., $\Omega_1 \cup \Omega_2$, Ω_3, Ω_1 and $\Omega_2 \cup \Omega_3$, respectively. In other words,

$$\begin{cases} \lim_{\boldsymbol{\sigma} \to \mathbf{c}} \varphi_{L=3}(\boldsymbol{\sigma}) = \varphi_{L=3}(\mathbf{c}) & \forall \boldsymbol{\sigma} \in \Omega_1 \cup \Omega_2 \\ \lim_{\boldsymbol{\sigma} \to \mathbf{c}} \varphi_{L=6}(\boldsymbol{\sigma}) = \varphi_{L=6}(\mathbf{c}) & \forall \boldsymbol{\sigma} \in \Omega_3 \\ \lim_{\boldsymbol{\sigma} \to \mathbf{c}} \varphi_{R=3}(\boldsymbol{\sigma}) = \varphi_{R=3}(\mathbf{c}) & \forall \boldsymbol{\sigma} \in \Omega_1 \\ \lim_{\boldsymbol{\sigma} \to \mathbf{c}} \varphi_{R=6}(\boldsymbol{\sigma}) = \varphi_{R=6}(\mathbf{c}) & \forall \boldsymbol{\sigma} \in \Omega_2 \cup \Omega_3; \end{cases} \tag{20}$$

therefore, $\varphi_{L=3}(\boldsymbol{\sigma})$ is continuous on $\Omega_1 \cup \Omega_2$, $\varphi_{L=6}(\boldsymbol{\sigma})$ is continuous on Ω_3, $\varphi_{R=3}(\boldsymbol{\sigma})$ is continuous on Ω_1 and $\varphi_{L=6}(\boldsymbol{\sigma})$ is continuous on $\Omega_2 \cup \Omega_3$.

Moreover, from Lemma 1 we have that $\lim_{\boldsymbol{\sigma} \to \mathbf{c}} \varphi_{L=3}(\boldsymbol{\sigma}) = \lim_{\boldsymbol{\sigma} \to \mathbf{c}} \varphi_{L=6}(\boldsymbol{\sigma}) = 0$ $\forall \mathbf{c} = [c_1, c_2] \mid c_2 = \omega_{23}(c_1)$ and $\lim_{\boldsymbol{\sigma} \to \mathbf{c}} \varphi_{R=3}(\boldsymbol{\sigma}) = \lim_{\boldsymbol{\sigma} \to \mathbf{c}} \varphi_{R=6}(\boldsymbol{\sigma}) = 0$ $\forall \mathbf{c} = [c_1, c_2] \mid c_2 = \omega_{12}(c_1)$. Therefore, we have the continuity also on the border ω_{23} for $\varphi_L(\boldsymbol{\sigma})$ and on the border ω_{12} for $\varphi_R(\boldsymbol{\sigma})$. Thus, $\varphi_L(\boldsymbol{\sigma})$ and $\varphi_R(\boldsymbol{\sigma})$ are continuous functions in the region $[-1,1]^2$, i.e., $\varphi_L \in \mathcal{C}^0([-1,1]^2)$ and $\varphi_R \in \mathcal{C}^0([-1,1]^2)$.

Finally, from the Theorem of Continuous Functions we know that the sum of a finite number of continuous functions is a continuous function. From the definitions in (14), $\varphi_1(\boldsymbol{\sigma})$, $\varphi_2(\boldsymbol{\sigma})$ and $\varphi_3(\boldsymbol{\sigma})$ are sums of $\varphi_{L=3}(\boldsymbol{\sigma})$, $\varphi_{L=6}(\boldsymbol{\sigma})$, $\varphi_{R=3}(\boldsymbol{\sigma})$ and $\varphi_{R=6}(\boldsymbol{\sigma})$, which are continuous. Therefore, also $\varphi_1(\boldsymbol{\sigma})$, $\varphi_2(\boldsymbol{\sigma})$ and $\varphi_3(\boldsymbol{\sigma})$ are all continuous functions in the region $[-1,1]^2$, i.e., $\varphi_1 \in \mathcal{C}^0([-1,1]^2)$, $\varphi_2 \in \mathcal{C}^0([-1,1]^2)$ and $\varphi_3 \in \mathcal{C}^0([-1,1]^2)$. Using the definitions in (14), $\varphi(\boldsymbol{\sigma})$ is a composition of $\varphi_1(\boldsymbol{\sigma})$, $\varphi_2(\boldsymbol{\sigma})$ and $\varphi_3(\boldsymbol{\sigma})$ which are continuous; therefore, also $\varphi(\boldsymbol{\sigma})$ is a continuous function in the region $[-1,1]^2$, i.e., $\varphi \in \mathcal{C}^0([-1,1]^2)$. ∎

Corollary 1: If the control inputs e and $\dot{e}$ to DI-IT2-FPID in Fig. 2 are continuous, then the control output v will also be continuous.

IV. CASE STUDY

A. Y6 Coaxial Tricopter UAV Control Scheme

For the dynamical simulations, the Y6 coaxial tricopter model is implemented in ROS environment and Gazebo simulator, which provides a seamless connection for the developed algorithms between the simulation and real-world applications. The overall structure of the closed-loop control scheme is illustrated in Fig. 6. It consists of three blocks in series: position controller, velocity controller and tricopter itself. For the velocity control, the nonlinear geometric controller on Euclidean group $\mathsf{SE}(3)$ is used [16]. The velocity controller computes the control input $\mathbf{u}$ from the UAV's attitude $\mathbf{o}$, its linear velocity $\mathbf{v}$, angular velocity in body frame $\boldsymbol{\omega}_B$ and desired linear velocity $\mathbf{v}^* = \begin{bmatrix} v_x^* & v_y^* & v_z^* \end{bmatrix}^T$. For the equations of motion of the UAV as well as the system parameters, the reader is kindly referred to [16].

If the absolute position of the tricopter $\mathbf{p} = \begin{bmatrix} x & y & z \end{bmatrix}^T$ is given by three Cartesian coordinates of its center of mass in the world frame and $\mathbf{p}^* = \begin{bmatrix} x^* & y^* & z^* \end{bmatrix}^T$ is the desired position of the UAV, then the position error is

$$\mathbf{e} = \begin{bmatrix} e_x & e_y & e_z \end{bmatrix}^T = \mathbf{p}^* - \mathbf{p}. \tag{21}$$

The position controller computes the desired linear velocity $\mathbf{v}^*$, in order to reach the desired position $\mathbf{p}^*$ from the current position $\mathbf{p}$. The position controller in Fig. 6 consists of three identical and independent DI-IT2-FPID sub-controllers for x, y and z axes. Each sub-controller takes the corresponding position error e and its time derivative $\dot{e}$, as the input, and returns the corresponding desired velocity v^*, as the output.
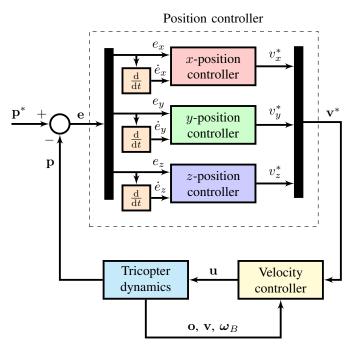

Fig. 6. Block diagram of the position controller for the tricopter UAV.

B. Trajectory Generation

In the simulation scenario, a square-wave 3D trajectory is chosen to test the stability and robustness of each controller with different PSs. The navigation of the UAV combines long and short straight lines path as well as hovering:

$$\begin{cases} x_k^* &= \left\lfloor \frac{k}{2} \right\rfloor \\ y_k^* &= 10 \left\lfloor \frac{(k-1) \bmod 4}{2} \right\rfloor \\ z_k^* &= 1, \end{cases} \tag{22}$$

where $k \in \mathbb{N}^+$ and $\lfloor \star \rfloor$ is the largest integer not greater than value $\star$. First, UAV hovers at $[0, 0, 1]$m. After that, UAV flies to the next way-point at $[1, 0, 1]$m and hovers for 10s before flying to the next way-point. This type of trajectory is often used in autonomous UAV mapping and exploration scenarios.

C. Simulation Results

Our main goal is to give a novel analysis for DI-IT2-FLC rather than compare its performance with other controllers. For the trajectory tracking problem, the following three PSs are investigated (for simplicity we have assumed $\alpha_1 = \alpha_2$):

1) PS-1: $\alpha_1 = \alpha_2 = 0.3$;
2) PS-2: $\alpha_1 = \alpha_2 = 0.5$;
3) PS-3: $\alpha_1 = \alpha_2 = 0.9$.

The 3D trajectory tracking of DI-IT2-FPID controllers with PS-1, PS-2 and PS-3 is shown in Fig. 7. The position responses of the designed DI-IT2-FPID controllers with PS-1, PS-2 and PS-3 are shown in Fig. 8. As can be seen from Fig. 8, the controller with PS-1 has an oscillatory behaviour, while the controller with PS-3 is relatively slow in converging to the desired value. On the other hand, the controller with PS-2 combines the characteristics of both controllers with PS-1 and PS-3; it is fast with smaller overshoot and no oscillations. The response properties are also given in Table II. As can be seen from Table II, DI-IT2-FPID with PS-1 has shorter rising time but longer settling time and overshoot, while DI-IT2-FPID with PS-3 has smaller overshoot but longer rise time. What is more, DI-IT2-FPID with PS-2 results in the lowest mean squared error value and settling time.
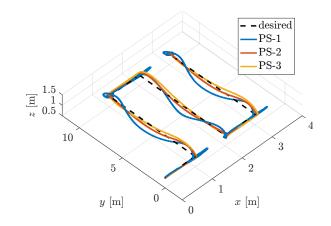

Fig. 7. 3D trajectory tracking results for DI-IT2-FPID position controllers with different values of α_1 and α_2.
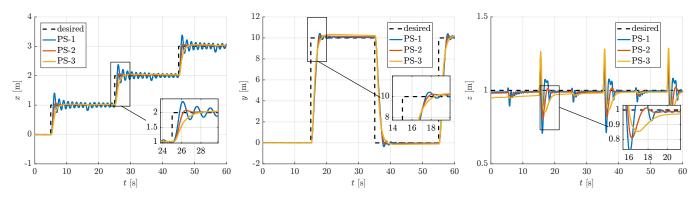
Fig. 8. Trajectory tracking for x, y and z axes of DI-IT2-FPID position controllers with different values of α_1 and α_2. The video is available at https://youtu.be/Eo2Cuk3Bo5Y.

On the other hand, from the analysis in Fig. 4 and Fig. 5, we expect that PSs with small values of α_1 and α_2, e.g., PS-1, will result in a more aggressive behaviour. Moreover, we expect that PSs with high values of α_1 and α_2, e.g., PS-3, will result in a smoother behaviour. Furthermore, we expect that PSs with intermediate values of α_1 and α_2, e.g., PS-2, will result in a moderate behaviour which is the case here. Therefore, it can be concluded that the simulation results match with the theoretical expectations.

V. CONCLUSION AND FUTURE WORK

In this paper, we have designed, deployed and analysed DI-IT2-FLC. We have presented the IT2-FLC design approach in which only two parameters have to be tuned. It has been shown that, by only tuning the FOU parameters, it is possible to design DI-IT2-FLC controller in a straightforward manner. Then, to validate these theoretical design and to show its simplicity, three DI-IT2-FPID controllers have been designed for the position control of the Y6 coaxial tricopter UAV. It is to be noted that two control loops exist in the UAV control: outer loop and inner loop. In each of them – assuming we design an FLC – we have a large number of parameters to be tuned. Therefore, the developed DI-IT2-FPID controller is suitable for UAV control, since it allows to reduce the number of parameters to be tuned. For the simulations, the DI-IT2-FPID controller is implemented in ROS and tested in Gazebo simulator. Finally, it has been shown that the theoretical analysis for DI-IT2-FLCs matches with the simulation results.

In the future, we will conduct real-time experiments with Y6 coaxial tricopter UAV using DI-IT2-FPID. Moreover, we will compare the performances of DI-IT2-FPID with other controllers in a variety of input noise and wind conditions.

TABLE II
PROPERTIES OF DIFFERENT CONTROLLERS.

DI-IT2-FPID controller	PS-1	PS-2	PS-3
Mean squared error, [m]	0.777	0.748	0.821
Overshoot, [m]	0.405	0.069	0.031
Rise time, [s]	0.80	1.18	3.32
Settling time (5%), [s]	-	1.71	2.53

REFERENCES

[1] R.-E. Precup and H. Hellendoorn, "A survey on industrial applications of fuzzy control," *Computers in Industry*, vol. 62, no. 3, pp. 213 – 226, 2011.

[2] J. Mendel, H. Hagras, W.-W. Tan, W. W. Melek, and H. Ying, *Introduction to Type-2 Fuzzy Logic Control: Theory and Applications*, 1st ed. Wiley-IEEE Press, 2014.

[3] H. Hagras, *Type-2 Fuzzy Logic Controllers: A Way Forward for Fuzzy Systems in Real World Environments*. Berlin, Heidelberg: Springer Berlin Heidelberg, 2008, pp. 181–200.

[4] H. Hagras, "A hierarchical type-2 fuzzy logic control architecture for autonomous mobile robots," *IEEE Transactions on Fuzzy Systems*, vol. 12, no. 4, pp. 524–539, Aug 2004.

[5] J. M. Mendel and R. I. B. John, "Type-2 fuzzy sets made simple," *IEEE Transactions on Fuzzy Systems*, vol. 10, no. 2, pp. 117–127, Apr 2002.

[6] J. M. Mendel and X. Liu, "Simplified Interval Type-2 Fuzzy Logic Systems," *IEEE Transactions on Fuzzy Systems*, vol. 21, no. 6, pp. 1056–1069, Dec 2013.

[7] T. Kumbasar, "A simple design method for interval type-2 fuzzy PID controllers," *Soft Computing*, vol. 18, no. 7, pp. 1293–1304, 2014.

[8] D. Wu and J. M. Mendel, "On the Continuity of Type-1 and Interval Type-2 Fuzzy Logic Systems," *IEEE Transactions on Fuzzy Systems*, vol. 19, no. 1, pp. 179–192, Feb 2011.

[9] O. Castillo and P. Melin, "A review on the design and optimization of interval type-2 fuzzy controllers," *Applied Soft Computing*, vol. 12, no. 4, pp. 1267 – 1278, 2012.

[10] H. Zhou and H. Ying, "A Method for Deriving the Analytical Structure of a Broad Class of Typical Interval Type-2 Mamdani Fuzzy Controllers," *IEEE Transactions on Fuzzy Systems*, vol. 21, no. 3, pp. 447–458, June 2013.

[11] T. Kumbasar, "Robust Stability Analysis and Systematic Design of Single-Input Interval Type-2 Fuzzy Logic Controllers," *IEEE Transactions on Fuzzy Systems*, vol. 24, no. 3, pp. 675–694, June 2016.

[12] J. Mendel, *Uncertain rule-based fuzzy logic system: introduction and new directions*. Upper Saddle River, NJ, USA, Prentice-Hall, 2001.

[13] W. Pedrycz and F. Gomide, *Notions and Concepts of Fuzzy Sets*. John Wiley & Sons, Inc., 2007, pp. 27–44.

[14] N. N. Karnik and J. M. Mendel, "Centroid of a type-2 fuzzy set," *Information Sciences*, vol. 132, no. 14, pp. 195 – 220, 2001.

[15] D. Wu and W. W. Tan, "A type-2 fuzzy logic controller for the liquid-level process," in *2004 IEEE International Conference on Fuzzy Systems*, vol. 2, July 2004, pp. 953–958 vol.2.

[16] A. Sarabakha and E. Kayacan, "Y6 Tricopter Autonomous Evacuation in an Indoor Environment Using Q-Learning Algorithm," in *IEEE 55th Conference on Decision and Control (CDC)*, Dec 2016, pp. 5992–5997.